A Geometrical Optics Model of Three Dimensional Scattering From a Rough Layer With Two Rough Surfaces

Nicolas Pinel, *Associate Member, IEEE*, Joel T. Johnson, *Fellow, IEEE*, and Christophe Bourlier, *Associate Member, IEEE*

***Abstract*—An asymptotic method is described for predicting the bistatic normalized radar cross section of a rough homogeneous layer made up of two rough surfaces. The model is based on iteration of the Kirchhoff approximation to calculate the fields scattered by the rough layer, and is reduced to the high-frequency limit in order to obtain numerical results rapidly. Shadowing effects, significant for large incidence or scattering angles, are taken into account through the use of shadowing functions. The model is applicable for moderate to large surface roughnesses having small to moderate slopes, and for both lossless and lossy inner media. It was validated for a rough layer with a rough surface over a perfectly flat surface in a preceding contribution. Here, the extension of the model to a rough layer with two rough surfaces is developed, and results are presented to validate the asymptotic model by comparison with a numerical reference method.**

***Index Terms*—Electromagnetic scattering by rough surfaces, multilayered media, physical optics, multistatic scattering.**

I. Introduction

THE aim of this paper is to extend the Kirchhoff approximation to the case of a rough layer with two rough interfaces, and to obtain a formulation of the bistatic normalized radar cross section (NRCS) in the high-frequency limit in the case where the upper and lower surfaces of the layer are uncorrelated. The model, which takes shadowing effects into account [1], [2], has been described in a recent publication [3] for a rough layer with a rough surface over a perfectly flat surface. Here, the extension of the model to a rough layer with two rough surfaces is developed. Numerical results are presented and compared with a reference numerical method to validate the model, for lossless as well as for lossy inner media.

Manuscript received February 26, 2009; revised June 09, 2009. First published December 28, 2009; current version published March 03, 2010.

N. Pinel and C. Bourlier are with the IREENA (Institut de Recherche en Electrotechnique et Electronique de Nantes Atlantique) Laboratory, Université Nantes Angers Le Mans, Polytech'Nantes, 44306 Nantes Cedex 3, France (e-mail: nicolas.pinel@gmail.com; christophe.bourlier@univ-nantes.fr).

J. T. Johnson is with the Department of Electrical and Computer Engineering and ElectroScience Laboratory, The Ohio State University, Columbus, OH 43210 USA (e-mail: johnson@ece.osu.edu).

Color versions of one or more of the figures in this paper are available online at http://ieeexplore.ieee.org.

Digital Object Identifier 10.1109/TAP.2009.2039306

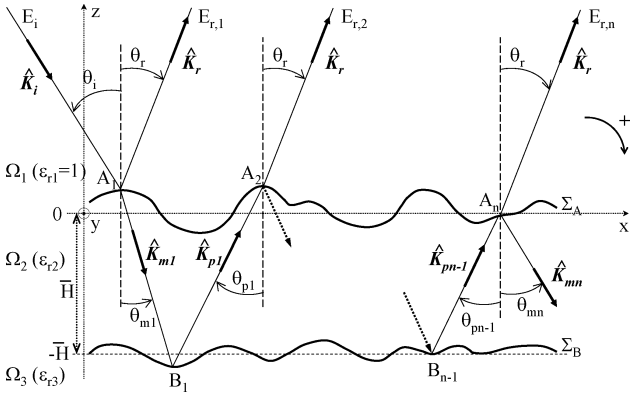

Fig. 1. Multiple scattering from a rough layer with two rough interfaces, represented in the plane $(\hat{\mathbf{x}}, \hat{\mathbf{z}})$. The points on the upper surface Σ_A are denoted as $\{A_1, A_2, \ldots, A_n\}$, whereas the points on the lower surface Σ_B are denoted as $\{B_1, B_2, \ldots, B_{n-1}\}$. θ_i is the elevation incidence angle, and θ_r is the elevation scattering angle in reflection, measured with respect to the vertical axis $\hat{\mathbf{z}}$. The positive sense is defined as clockwise.

II. Calculation of the Scattered Fields Derived With the KA and the MSP

A. Problem Presentation

The studied system (see Fig. 1) is made up of a rough layer with two rough interfaces (with an upper interface Σ_A and a lower interface Σ_B), separating homogeneous media Ω_α, with $\alpha = \{1, 2, 3\}$. Each of the three media Ω_α, with relative permittivity $\epsilon_{r\alpha}$, is assumed to be non magnetic (relative permeability $\mu_r = 1$). The same notations as in [3] are used.

As for a flat lower interface [3], in order to calculate the fields $\mathbf{E_{r,1}}$ and $\mathbf{E_{r,2}}$, the Kirchhoff approximation (KA) (which is sometimes also called physical optics approximation, or tangent plane approximation) is iterated for each scattering inside the rough layer, i.e., on the interaction among interfaces (and not for multiple scattering from the same rough interface). The formulation is further simplified by applying the method of stationary phase (MSP) for each scattering point inside the rough layer. Using these two approximations in the calculation of scattered fields (note the MSP could have been applied only when calculating the NRCS, but applying the MSP for the scattered fields allows simpler calculations), simplified expressions for $\mathbf{E_{r,1}}$ and $\mathbf{E_{r,2}}$ can be obtained: in the case of 1-D surfaces, with 1 numerical integration for $\mathbf{E_{r,1}}$, and 5 fold numerical integrations for $\mathbf{E_{r,2}}$ [4]. Here, for the case of 2-D surfaces, the number of numerical integrations is doubled as shown in what follows.

B. Fields Scattered by the Rough Layer

Under the KA, the derivation of the first-order scattered field $\mathbf{E_{r,1}}$, corresponding to the scattering from a single rough surface, is well-known and developed in [3]. The higher-order scattered fields ($\mathbf{E_{r,2}}, \mathbf{E_{r,3}}$, etc.) are obtained by the same way as for the flat lower interface case [3], i.e., by iterating the KA at each scattering among interfaces. The main difference with the flat case concerns the scattering from the lower interface, where the KA must be applied to model lower surface roughness scattering. Thus, the second-order scattered field in reflection $\mathbf{E^{\infty}_{r,2}}$ is given under the MSP by the relation

$$\begin{aligned}\frac{\mathbf{E^{\infty}_{r,2}}(\mathbf{R})}{E_0} = {} & \frac{-ik_1k_2^2\, e^{ik_1R}}{(2\pi)^5 R} \\ & \times \int \frac{d\mathbf{k_{m1}}\, d\mathbf{k_{p1}}}{-k_{m1z}\, k_{p1z}}\, d\mathbf{r_{A_1}} d\mathbf{r_{B_1}} d\mathbf{r_{A_2}} \\ & \bar{F}_{t,21}(\mathbf{K_{p1}}, \mathbf{K_r}) \\ & \times \bar{F}_r(\mathbf{K_{m1}}, \mathbf{K_{p1}}) \times \bar{F}_{t,12}(\mathbf{K_i}, \mathbf{K_{m1}}) \\ & e^{i(\mathbf{K_i}\cdot\mathbf{R_{A_1}} + \mathbf{K_{m1}}\cdot\mathbf{R_{A_1B_1}} + \mathbf{K_{p1}}\cdot\mathbf{R_{B_1A_2}} - \mathbf{K_r}\cdot\mathbf{R_{A_2}})} \\ & \Xi_t(\mathbf{R_{A_1}})\, \Xi_r(\mathbf{R_{B_1}})\, \Xi_t(\mathbf{R_{A_2}}) \end{aligned} \quad (1)$$

with $\mathbf{R_{B_1A_2}} = \mathbf{R_{A_2}} - \mathbf{R_{B_1}}$ and Ξ indicate surface illumination functions. The calculation of $\mathbf{E^{\infty}_{r,2}}$ then implies 2×5 fold numerical integrations.

By using the same principle for the higher orders, i.e., by iterating the KA at each scattering among interfaces, and using the MSP, it is possible to obtain the expressions of the scattered fields in reflection $\mathbf{E^{\infty}_{r,n}}$ at any order $n \in \mathbb{N}^*$. Nevertheless, their expression is long and is consequently not given here.

III. NRCS in the High-Frequency Limit

A general description of the NRCS in the high-frequency limit can be found in Section III of [3].

A. Expression of the Second-Order Contribution

The first-order NRCS in reflection $\bar{\sigma}_{r,1}(\mathbf{K_r}, \mathbf{K_i})$ corresponds to the NRCS in reflection from a single rough interface. Under the KA and the MSP, and by using the Geometric Optics Approximation (GOA), $\bar{\sigma}_{r,1}(\mathbf{K_r}, \mathbf{K_i})$ is well-known [5], [6], and expressed by [3, Eq. (7)].

For the second-order contribution $\bar{\sigma}_{r,2}(\mathbf{K_r}, \mathbf{K_i})$, the principle is the same as for 1-D surfaces (see [4, Subsection 3.1.1]), and the expression is similar to the flat lower interface case. The main difference comes from the scattering in reflection from the rough lower interface. Thus, the second-order NRCS $\bar{\sigma}_{r,2}$ can be written as

$$\begin{aligned}\bar{\sigma}_{r,2}(\mathbf{K_r}, \mathbf{K_i}) = {} & \frac{1}{\cos\theta_i} \int \sin\theta_{m1} d\theta_{m1} d\phi_{m1} \sin\theta_{p1} d\theta_{p1} d\phi_{p1} \\ & |\bar{F}_{t,21}(\mathbf{K_{p1}}, \mathbf{K_r}) \times \bar{F}_r(\mathbf{K_{m1}}, \mathbf{K_{p1}}) \\ & \times \bar{F}_{t,12}(\mathbf{K_i}, \mathbf{K_{m1}})|^2 \\ & \frac{p_s\left(\boldsymbol{\gamma}^{\mathbf{0(t)}}_{\mathbf{A_1}}\right)}{\left|\hat{k}_{m1z} - \frac{k_1}{k_2}\hat{k}_{iz}\right|^2}\, S_{12}\left(\mathbf{K_i}, \mathbf{K_{m1}} | \boldsymbol{\gamma}^{\mathbf{0(t)}}_{\mathbf{A_1}}\right) \\ & \frac{p_s\left(\boldsymbol{\gamma}^{\mathbf{0(r)}}_{\mathbf{B_1}}\right)}{\left|\hat{k}_{p1z} - \hat{k}_{m1z}\right|^2}\, \S_{22}\left(\mathbf{K_{m1}}, \mathbf{K_{p1}} | \boldsymbol{\gamma}^{\mathbf{0(r)}}_{\mathbf{B_1}}\right) \\ & \frac{p_s\left(\boldsymbol{\gamma}^{\mathbf{0(t)}}_{\mathbf{A_2}}\right)}{\left|\hat{k}_{rz} - \frac{k_2}{k_1}\hat{k}_{p1z}\right|^2}\, S_{21}\left(\mathbf{K_{p1}}, \mathbf{K_r} | \boldsymbol{\gamma}^{\mathbf{0(t)}}_{\mathbf{A_2}}\right) \end{aligned} \quad (2)$$

with $\boldsymbol{\gamma}^{\mathbf{0(t)}}_{\mathbf{A_1}} = (\gamma^{0(t)}_{A_1,x}, \gamma^{0(t)}_{A_1,y})$, $\boldsymbol{\gamma}^{\mathbf{0(r)}}_{\mathbf{B_1}} = (\gamma^{0(r)}_{B_1,x}, \gamma^{0(r)}_{B_1,y})$, and $\boldsymbol{\gamma}^{\mathbf{0(t)}}_{\mathbf{A_2}} = (\gamma^{0(t)}_{A_2,x}, \gamma^{0(t)}_{A_2,y})$ given by

$$\gamma^{0(t)}_{A_1,x,y} = -(k_{m1x,y} - k_{ix,y})/(k_{m1z} - k_{iz}) \quad (3)$$

$$\gamma^{0(r)}_{B_1,x,y} = -(k_{p1x,y} - k_{m1x,y})/(k_{p1z} - k_{m1z}) \quad (4)$$

$$\gamma^{0(t)}_{A_2,x,y} = -(k_{rx,y} - k_{p1x,y})/(k_{rz} - k_{p1z}). \quad (5)$$

Here p_s refers to the rough surface slope probability density function; use of the p_s for the upper or lower interface is apparent from the argument of the function. The bistatic average shadowing function in reflection $S_{22}(\mathbf{K_{m1}}, \mathbf{K_{p1}} \mid \boldsymbol{\gamma}^{\mathbf{0(r)}}_{\mathbf{B_1}})$ is given by [3, Eq. (17)], and the bistatic average shadowing functions in transmission are given by $S_{12}(\mathbf{K_i}, \mathbf{K_{m1}} \mid \boldsymbol{\gamma}^{\mathbf{0(t)}}_{\mathbf{A_1}}) = B[1 + \Lambda(\mathbf{K_i}), 1 + \Lambda(\mathbf{K_{m1}})]$, and $S_{21}(\mathbf{K_{p1}}, \mathbf{K_r} | \boldsymbol{\gamma}^{\mathbf{0(t)}}_{\mathbf{A_2}}) = B[1 + \Lambda(\mathbf{K_{p1}}), 1 + \Lambda(\mathbf{K_r})]$, where B is the Beta function (also called the Eulerian integral of the first kind). The terms $F_{t,21}(\mathbf{K_{p1}}, \mathbf{K_r})$, $F_r(\mathbf{K_{m1}}, \mathbf{K_{p1}})$, and $F_{t,12}(\mathbf{K_i}, \mathbf{K_{m1}})$ are polarization square matrices of dimension 2, given by [3, Eq. (22)], their components being given by [3, Eqs. (23) and (24)] for reflection and transmission, respectively. The wave vectors $\mathbf{K_i}$, $\mathbf{K_r}$, $\mathbf{K_{m1}}$, and $\mathbf{K_{p1}}$ are given by $\mathbf{K_i} = k_1\hat{\mathbf{K}}_\mathbf{i}$, $\mathbf{K_r} = k_1\hat{\mathbf{K}}_\mathbf{r}$, $\mathbf{K_{m1}} = k_2\hat{\mathbf{K}}_\mathbf{m1}$, and $\mathbf{K_{p1}} = k_2\hat{\mathbf{K}}_\mathbf{p1}$, with k_1 and k_2 the wavenumbers inside Ω_1 and Ω_2, respectively. The normalized wave vectors $\hat{\mathbf{K}}_\mathbf{i}$, $\hat{\mathbf{K}}_\mathbf{r}$, $\hat{\mathbf{K}}_\mathbf{m1}$, and $\hat{\mathbf{K}}_\mathbf{p1}$ are given by [3, Eqs. (1a)–(1d)]. The terms $\hat{k}_{iz}$, $\hat{k}_{rz}$, $\hat{k}_{m1z}$, and $\hat{k}_{p1z}$ are the vertical components (i.e., the projections with respect to the axis $\hat{\mathbf{z}}$) of $\hat{\mathbf{K}}_\mathbf{i}$, $\hat{\mathbf{K}}_\mathbf{r}$, $\hat{\mathbf{K}}_\mathbf{m1}$, and $\hat{\mathbf{K}}_\mathbf{p1}$, respectively.

It can be noticed that the computation of $\bar{\sigma}_{r,2}(\mathbf{K_r}, \mathbf{K_i})$ implies four fold numerical integrations, which should in general require rather long computing time. Nevertheless, the method being geometric-based, it is possible to optimize the numerical integrations, as described in [7, Section 3.A]. Thus, a reasonable computing time can be achieved, as described in Section IV-A.

Higher-order NRCS quantities can be calculated in a similar manner, but are not considered here.

B. Model Validity Domains and Properties

As for the flat lower interface case [3], the validity domains of the model are similar to those in the 2-D problem (with 1-D surfaces): see [7, Section 2.C] and [3, Section III.B]. The main difference with [3] comes from the fact that the constraints also concern the lower rough interface. Based on the iteration of the Kirchhoff approximation (KA) to compute scattering interactions among the interfaces of the rough layer and the high frequency approximation, the overall approach has the validity domain of the geometric optics approximation (GOA). That is why

this method is called the geometric optics approximation for a rough layer and is denoted GOA.

The model has the same general properties as for the flat lower interface case [3], see second paragraph of Subsection III-B. In particular, the model in itself, as based on the GOA, cannot deal with lossy media *a priori*. Still, by using exactly the same approach as for the 2-D case (see [4, Section 7]), as it will be shown here in the following numerical results, lossy media can be taken into account *a posteriori* and give satisfying results. To do so, the power propagation losses $\mathcal{A}$ can be evaluated by considering flat interfaces, $\mathcal{A} \simeq \mathcal{A}_{\text{flat}}$. Then, in the particular case of normal incidence $\theta_i = 0$, the losses correspond to a back-and-forth of the wave inside the lossy layer of mean thickness $\bar{H}$. The associated imaginary part of the phase $\Delta\phi''$ is given by

$$\Delta\phi''(\theta_i = 0) = k_0 2\bar{H}\Im m(\sqrt{\underline{\epsilon}_{r2}}) \tag{6}$$

with k_0 the wavenumber inside the vacuum, $\underline{\epsilon}_{r2}$ the complex relative permittivity of the lossy layer, and $\Im m(\cdots)$ the imaginary part operator. As a result, the power propagation losses are given by

$$\mathcal{A} \simeq \mathcal{A}_{\text{flat}} = \exp[-2\Delta\phi''(\theta_i = 0)]. \tag{7}$$

In the next section, asymptotic model (GOA) predictions of the first two order contributions of the NRCS, $\bar{\sigma}^{\text{tot}}_{r,1} = \bar{\sigma}_{r,1}$ and $\bar{\sigma}^{\text{tot}}_{r,2} = \bar{\sigma}_{r,1} + \bar{\sigma}_{r,2}$, are compared with a reference numerical method for validation. The validation concerns the second-order contribution, as the first-order contribution $\bar{\sigma}^{\text{tot}}_{r,1} = \bar{\sigma}_{r,1}$, corresponding to the scattering in reflection from a single rough surface, is well-known.

IV. Numerical Results: GOA Validation

A. Numerical Reference Method

The same numerical reference method as in [3] (see [8]–[13] for additional information) is used, as this code is capable of treating both flat and rough lower layer boundaries.

The results to be illustrated consider a layer of relative permittivity $\epsilon_{r2} = 3$ or $\epsilon_{r2} = 3 + i0.05$ or $\epsilon_{r2} = 3 + i0.01$, above a rough perfectly conducting boundary ($\epsilon_{r3} = i\infty$). The surface profiles were generated as independent realizations of a Gaussian stochastic process with an isotropic Gaussian correlation function, and the cases considered used identical surface statistics (but independent surface realizations) for the upper and lower interfaces. Three roughness cases are considered: rms height 0.1875λ or 0.25λ or 0.375λ and correlation length 1.768λ, corresponding to rms slope 0.15 or 0.2 or 0.3, respectively. A mean distance of 2.41 free space wavelengths between the layers was used in the numerical method.

The reference numerical method used surface sizes of 24 by 24 free space wavelengths, discretized into 256 by 256 points for a total of 393216 unknowns in the matrix equation (4 or 2 unknowns for each point on the upper and lower interfaces, respectively). A total of 32 surface realizations (sufficient to achieve mean NRCS estimates accurate to within approximately 2 dB) were used in each simulation, with the required computations performed on parallel computing resources at the Maui High Performance Computing Center. Results for a single surface realization used 8 processors as described in [3], and required approximately 8 hours of CPU time. By comparison, the typical CPU time to compute the GOA is of the order of 25 seconds on a standard office computer using MATLAB for each observation configuration (θ_r, ϕ_r), for a total of 15 minutes for each simulation presented in the following.

In the comparisons to be shown, the incident wave is linearly polarized with an incident elevation angle θ_i of 0° (normal incidence), 20° or 40°, and the incident azimuth angle is always $\phi_i = 0°$. The numerical results present the n-th order total NRCS in reflection $\bar{\sigma}^{\text{tot}}_{r,n}$ for HH, HV, VH, VV polarizations (the first term representing the polarization of the scattered wave, and the second term the polarization of the incident wave) and in either the plane of incidence ($\phi_r = 0$) or in scattering planes rotated azimuthally with respect to the plane of incidence (ϕ_r not zero). More precisely, about the GOA, the first two order contributions $n = 1$ (reported as "1" in the legend of the figures) and $n = 2$ (reported as '1 + 2' in the legend of the figures) of $\bar{\sigma}^{\text{tot}}_{r,n}$ are computed for the asymptotic model. For the numerical reference method, $n = 1$ and $n = 2$ are computed, together with the total contribution $n \to \infty$ which takes all the significant contributions into account (reported as "Tot" in the legend of the figures). It must be noted that under the numerical reference method, it was checked that for all cases (and especially when the rms height is 0.1875λ), the coherent contribution is negligible by comparison with the incoherent contribution, which is a necessary condition for the applicability of the GOA.

B. Simulation Results

For all configurations, it is recalled that the layer mean thickness $\bar{H} = 2.41\lambda$, and the lower medium Ω_3 is perfectly conducting, $\epsilon_{r3} = i\infty$. Moreover, for the first configuration to be simulated, for both surfaces the rms height $\sigma_h = 0.1875\lambda$, which makes the rms slope $\sigma_s = 0.15$, and the layer is of relative permittivity $\epsilon_{r2} = 3$.

Fig. 2 presents numerical results for scattering in the plane of incidence (azimuth angle $\phi_r = 0°$) for an incidence angle $\theta_i = 0°$. For the GOA, the first-order contribution $\bar{\sigma}^{\text{tot}}_{r,1} = \bar{\sigma}_{r,1}$ is plotted as a black line with circles. The second-order contribution $\bar{\sigma}^{\text{tot}}_{r,2} = \bar{\sigma}_{r,1} + \bar{\sigma}_{r,2}$ is plotted as a dotted line with plus signs. For the numerical simulations of the reference numerical method, results are presented in all polarizations for normal incidence, but were computed only in HH and VH polarizations for this case. Then, to plot VH and VV polarizations, the following symmetries of the bistatic NRCS for a normally incident plane wave were used

$$\sigma^r_{\text{VH}}(\theta_i = 0, \theta_r, \phi_r + 90°) = \sigma^r_{\text{VV}}(\theta_i = 0, \theta_r, \phi_r) \tag{8}$$

$$\sigma^r_{\text{HV}}(\theta_i = 0, \theta_r, \phi_r + 90°) = \sigma^r_{\text{HH}}(\theta_i = 0, \theta_r, \phi_r). \tag{9}$$

The contribution from the upper interface alone obtained from the numerical method, corresponding to $\bar{\sigma}^{\text{tot}}_{r,1} = \bar{\sigma}_{r,1}$, is plotted as a solid line. The result after one iteration of the method, corresponding to $\bar{\sigma}^{\text{tot}}_{r,2} = \bar{\sigma}_{r,1} + \bar{\sigma}_{r,2}$, is plotted as a dash-dot line, and the result after many iterations, corresponding to $\bar{\sigma}^{\text{tot}}_{r,n} \simeq \bar{\sigma}^{\text{tot}}_{r,\infty}$, is plotted as a dashed line.

In co-polarizations HH and VV, the first two order contributions of the total NRCS $\bar{\sigma}^{\text{tot}}_{r,1}$ and $\bar{\sigma}^{\text{tot}}_{r,2}$ of the GOA have the same basic properties as in the 2-D problem (see [4, Section 6] and [7, Section 3.C]). The second-order total NRCS $\bar{\sigma}^{\text{tot}}_{r,2}$ contributes for all scattering angles, and is much larger than that of the first-order NRCS $\bar{\sigma}^{\text{tot}}_{r,1}$. Similarly as for the 2-D problem, the

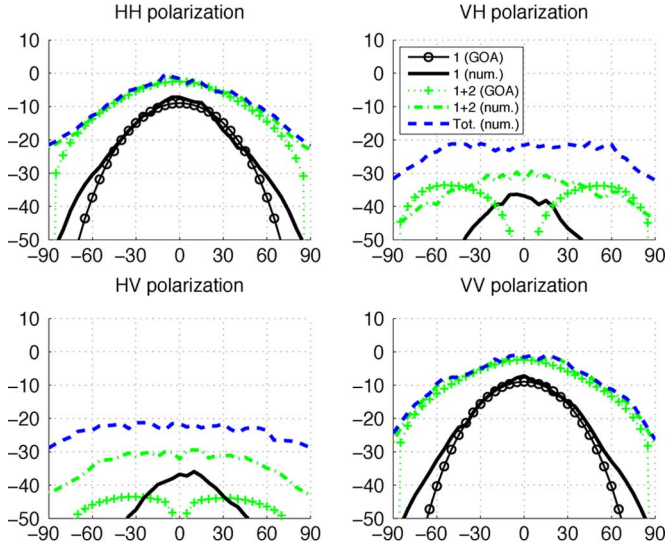

Fig. 2. Simulation of the first two total NRCSs $\bar{\sigma}_{r,1}^{\mathrm{tot}}$ and $\bar{\sigma}_{r,2}^{\mathrm{tot}}$ in dB scale, with respect to the observation angle θ_r in the plane of incidence (azimuth angle $\phi_r = 0°$), for an incidence elevation angle $\theta_i = 0°$. The rough surfaces have same rms slope $\sigma_s = 0.15$, the layer is of mean thickness $\bar{H} = 2.41\lambda$ with relative permittivity $\epsilon_{r2} = 3$, and the lower medium is perfectly conducting ($\epsilon_{r3} = i\infty$).

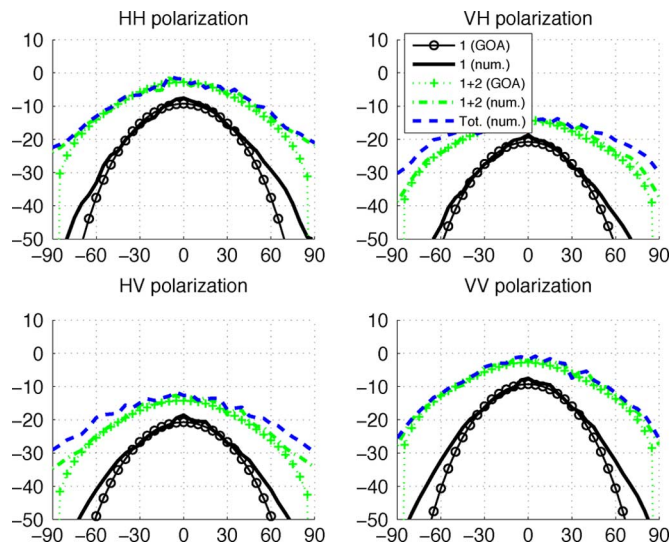

Fig. 3. Same simulations as in Fig. 2, but with an azimuth angle $\phi_r = 15°$.

case without shadowing effects (which is not represented here for the sake of clarity of the figure) diverges for observation angles $|\theta_r| \gtrsim 80°$: this highlights the relevance of taking shadowing into account for grazing angles. In cross-polarizations VH and HV, as expected by the first-order KA, the first-order NRCS $\bar{\sigma}_{r,1}^{\mathrm{tot}}$ of the GOA has a negligible contribution compared to the second-order contribution $\bar{\sigma}_{r,2}^{\mathrm{tot}}$.

For HH polarization, the comparison with the reference numerical method shows a very good agreement for $\bar{\sigma}_{r,1}^{\mathrm{tot}}$, which corresponds to the scattering from the upper surface when no lower layer is present. The differences that appear for grazing angles, $|\theta_r| \gtrsim 60°$, are likely impacted by the finite surface size as well as the limitations of the GOA (more precisely, the neglect of the multiple scattering from the same interface effect) for this region. Very good agreement is also observed for the second-order contribution $\bar{\sigma}_{r,2}^{\mathrm{tot}}$; significant differences are observed only for grazing angles, $|\theta_r| \gtrsim 75°$, also likely impacted by the finite surface size as well as limitations of the GOA. Indeed, the observed differences in co-polarizations are very similar to the ones obtained for a 2-D problem: for instance, see [7, Fig. 2] for a similar configuration. The result of the numerical method for many iterations highlights that for all scattering angles for these surfaces, there is no significant difference with the first iteration $\bar{\sigma}_{r,2}^{\mathrm{tot}}$, which means that $\bar{\sigma}_{r,2}^{\mathrm{tot}}$ is sufficient to quantify the scattering process. This result is in agreement with observations made for a 2-D problem (see [7, Section 3.B]). Thus, in co-polarization, the second-order contribution $\bar{\sigma}_{r,2}^{\mathrm{tot}}$ of the GOA model can correctly quantify the scattering process for moderate observation angles, $|\theta_r| \lesssim 75°$ (the difference being likely attributed to the neglect of multiple scattering effects). The same general comments and conclusions can be drawn for VV polarization.

For cross-polarization VH, the comparison of the GOA with the reference method highlights an underestimation for the second-order contribution $\bar{\sigma}_{r,2}^{\mathrm{tot}}$ for moderate observation angles θ_r. This may be attributed to multiple scattering from the same interface effect or possibly to finite surface size effects, although such effects would likely not be major contributors for angles within 30 degrees scattering angle. The total scattering coefficient computed from the reference method shows larger contributions for all θ_r. The same general comments and conclusions can be drawn for HV polarization, where the GOA underestimates $\bar{\sigma}_{r,2}^{\mathrm{tot}}$ for all angles θ_r.

Nevertheless, as for the flat lower interface case, for this rms slope, as soon as the azimuthal scattering direction ϕ_r moves away from 0 degrees, the agreement of the GOA with the reference numerical method is good both in co- and cross-polarizations. This is illustrated in Fig. 3 for $\phi_r = 15°$: for the second-order contribution $\bar{\sigma}_{r,2}^{\mathrm{tot}}$, in VH and HV polarizations the GOA is in very good agreement with the numerical method, for scattering angles $|\theta_r| \lesssim 75°$. The agreement of the GOA with the reference method is improved in this comparison compared to that for the plane-of-incidence, since first-order scattering effects are more important in both polarizations, leading to a lower relative contribution of the multiple scattering effects. Moreover, the difference between the total scattering coefficient $\bar{\sigma}_{r,\infty}^{\mathrm{tot}}$ and $\bar{\sigma}_{r,2}^{\mathrm{tot}}$ in the numerical method becomes weak here, and is significant only for scattering angles $|\theta_r| \gtrsim 45°$ for both cross-polarizations. In HH and VV co-polarizations, the same general remarks and conclusions as for $\phi_r = 0$ are applicable, with the agreement of the GOA being very good for moderate scattering angles.

Fig. 4 presents results for the same parameters as in Fig. 2, but for azimuth angle $\phi_r = 105°$. As $\phi_r = 105°$ is a 90° azimuthal rotation from the results of Fig. 3 where $\phi_r = 15°$, the numerical results for co-polarizations are similar to those for cross-polarization obtained in Fig. 3 and vice-versa. Therefore, co-pol and cross-pol results here can largely be interpreted in the same manner as used for cross-pol and co-pol results, respectively.

Other comparisons (not presented here) for various rotations of the scattering plane (i.e., ϕ_r values) investigated whether both

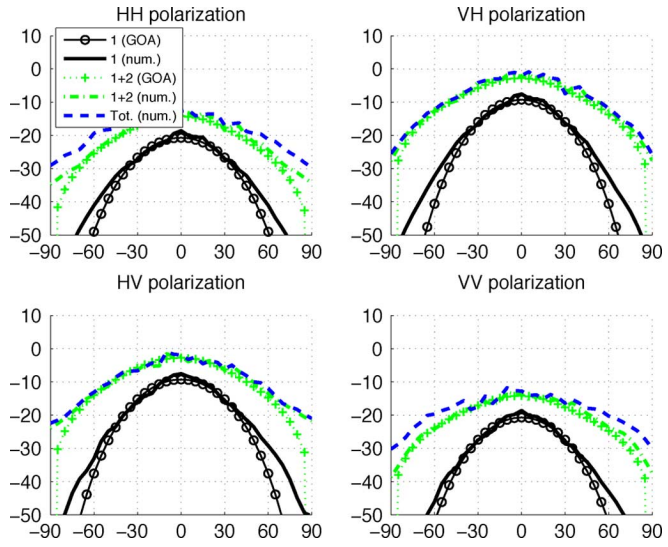

Fig. 4. Same simulations as in Fig. 2, but with an azimuth angle $\phi_r = 105°$.

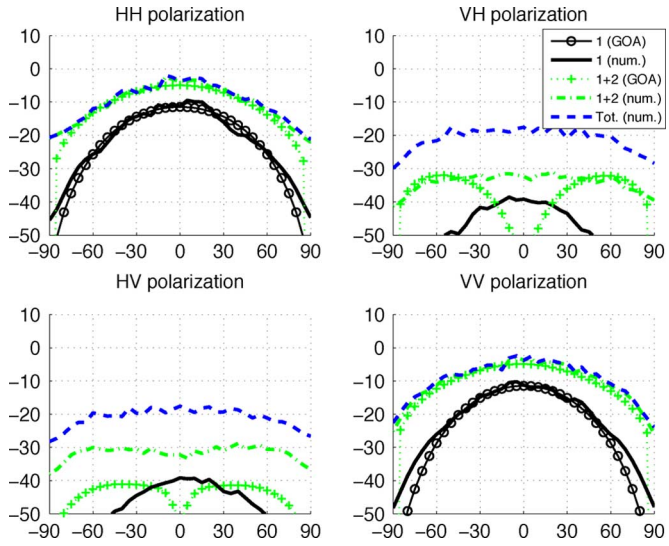

Fig. 5. Same simulations as in Fig. 2, but with surfaces of rms slope $\sigma_s = 0.2$.

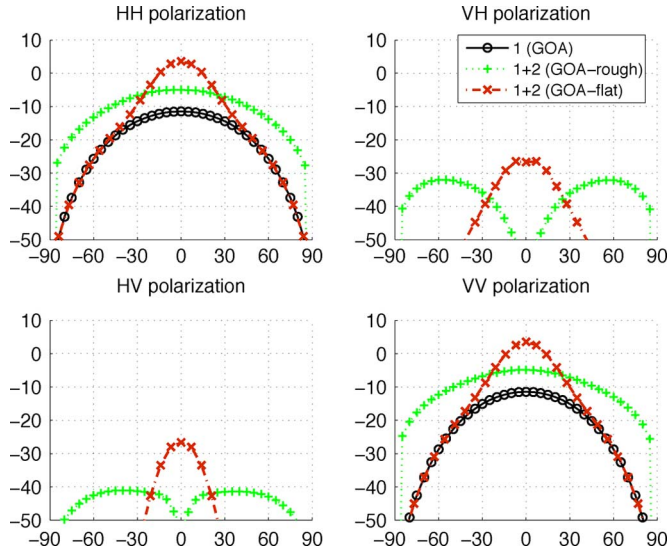

Fig. 6. Same simulation parameters as in Fig. 5, but only the GOA is represented here, for which a comparison is made between the cases of a rough and a flat lower interface (second-order contribution $\bar{\sigma}_{r,2}$).

the GOA and the reference numerical method captured the appropriate symmetries of the bistatic NRCS for a normally incident plane wave, given by (8) and (9). Both methods were found to achieve these symmetries.

Fig. 5 presents comparisons for the parameters of Fig. 2, but with surfaces of rms slope $\sigma_s = 0.2$. While the surface correlation length L_c remains unchanged, the reference numerical method used a surface RMS height $\sigma_h = 0.25\lambda$ to achieve $\sigma_s = 0.2$. The numerical results are similar to those of Fig. 2, the agreement of the GOA with the reference numerical method being at least as good as in the previous configuration. The results for azimuthal rotations of ϕ_r lead to the same general results and comments. Thus, the same general conclusions can be drawn. Moreover, a similar scenario, but with a layer mean thickness $\bar{H} = 5.41\lambda$ was tested, leading to very similar quantitative results on the numerical method, which confirms the general property of the GOA of being independent of the layer mean thickness for lossless inner media Ω_2.

A comparison (not presented here) between the in-plane co-polarized 3-D results and the 2-D results of the GOA model was made for the same roughness statistics and layer dielectric properties. The comparison showed that for the first-order contribution $\bar{\sigma}_{r,1}$, the ratio $C_{r,1}$ of the 3-D case to the 2-D case is weak (less than 1 dB) for moderate incidence angles and moderate scattering angles. More generally, it can be shown that this ratio is given for a Gaussian height pdf and without shadowing effects by the general relation

$$C_{r,1} = \frac{1}{\cos\theta_r + \cos\theta_i} \times \frac{1}{\sigma_s\sqrt{2\pi}}. \tag{10}$$

For the second-order contribution $\bar{\sigma}_{r,2}$, the ratio $C_{r,2}$ cannot be expressed from a simple mathematical formula. Nevertheless, by comparing the numerical results, it can be noticed that the two curves have the same general behavior. For this typical configuration with $\theta_i = 0$, the ratio $C_{r,2}$ is practically nearly constant and of the order of -2.3 dB in this case. However, this ratio decreases for increasing rms slope σ_s, and significantly varies with θ_r for $\theta_i \neq 0$.

Fig. 6 presents comparisons for the parameters of Fig. 5, but the results make comparisons of the GOA model for flat and rough lower interfaces, as plotted in [3, Fig. 2]. Then, for the second-order contribution $\bar{\sigma}^{\text{tot}}_{r,2}$, the GOA model with the case of a flat lower interface is plotted in dash-dot line with crosses. Similarly as for the 2D case (see [4, Section 6]), significant differences between a rough and a flat lower interface appear. For a flat lower interface, the second-order contribution is concentrated around the specular direction $\{\theta_r = +\theta_i, \phi_r = +\phi_i\}$. Indeed, as the lower interface is flat, the energy incident on the lower interface is not scattered in all directions like for the rough case but reflected in the specular direction. On the contrary, for a rough lower interface, the second-order contribution is lower in and around the specular direction $\{\theta_r = +\theta_i, \phi_r = +\phi_i\}$, and is more uniformly distributed in all scattering angles. Indeed, the rough lower interface scatters energy in all directions.

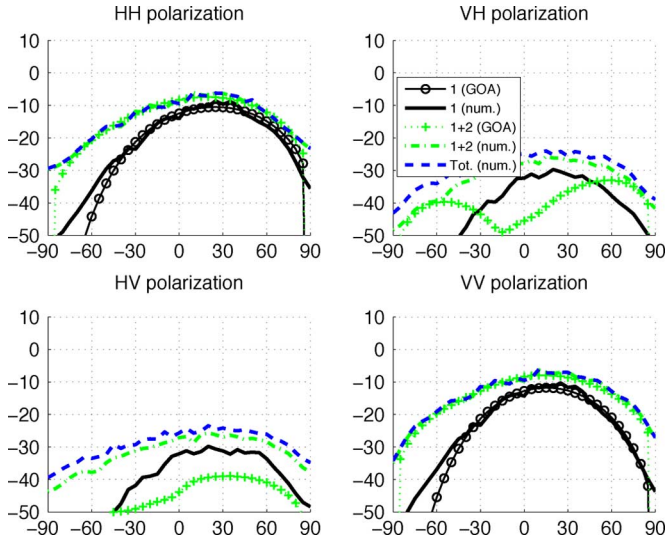

Fig. 7. Same simulations as in Fig. 5, but with an incidence elevation angle $\theta_i = 20°$ and an inner relative permittivity $\epsilon_{r2} = 3 + i0.05$.

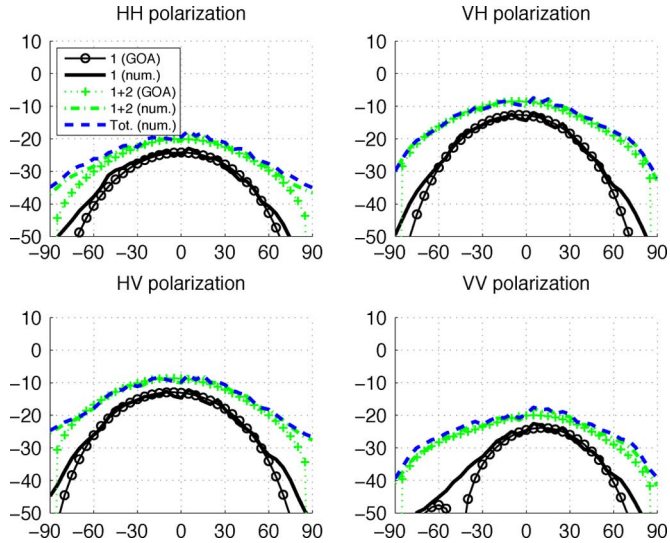

Fig. 8. Same simulations as in Fig. 7, but with an azimuth angle $\phi_r = 105°$.

Fig. 7 presents comparisons with the numerical method for the parameters of Fig. 5, but with an incidence angle $\theta_i = 20°$ and an inner relative permittivity $\epsilon_{r2} = 3+i0.05$. The model itself cannot deal with lossy media *a priori*, but the effect of lossy media can be taken into account *a posteriori*. Then, the lossy inner medium is taken into account in the GOA as described in [4, Section 7]. The results show the same general behavior of the GOA as in the preceding configuration. The results for the case without shadowing effects (not presented here for the sake of clarity of the figure) again diverge for grazing θ_r. The results of the GOA are compared with the reference numerical method for all polarizations (HH, VH, HV, VV). In co-polarizations HH and VV, the first-order contribution $\bar{\sigma}^{\rm tot}_{r,1}$ highlights a good agreement of the GOA with the reference method. Again differences that appear for larger θ_r values, and in particular for $\theta_r < -45°$, can be attributed to the limitations of the GOA as well as tapered wave effects at the larger angles. The second-order contribution $\bar{\sigma}^{\rm tot}_{r,2}$ highlights a good agreement of the GOA with the reference method for $|\theta_r| \lesssim 85°$. As in Figs. 2 and 5, results from the reference numerical method highlight that for all scattering angles θ_r, the higher orders are negligible: the second-order $\bar{\sigma}^{\rm tot}_{r,2}$ is enough to quantify the scattering phenomenon.

In cross-polarizations VH and HV, results from the GOA confirm that $\bar{\sigma}^{\rm tot}_{r,1}$ has a negligible contribution, while $\bar{\sigma}^{\rm tot}_{r,2}$ has a relatively low contribution. The reference method again shows appreciable contributions for $\bar{\sigma}^{\rm tot}_{r,1}$ that are impacted by the tapered wave and are likely to be overestimates of the true scattering. Once again, the GOA underestimates cross-polarized scattering, especially for moderate θ_r. This is likely due to the impact of multiple scattering on the upper interface, which plays a significant role generally in cross-polarized scattering. Still, a rather good agreement is found in VH polarization for relatively high scattering angles, $|\theta_r| \gtrsim 60°$. The results of the reference method for higher orders show that the second-order contribution when computed exactly underestimates the total scattering only slightly for these surface statistics and incidence angles.

Fig. 8 presents numerical results for the same parameters as in Fig. 7, but for a rotated scattering plane at azimuth angle $\phi_r = 105°$. Again, the main changes from $\phi_r = 0°$ appear in co-polarization. Overall, a good agreement is found with the reference method because multiple scattering effects are less important when compared to first-order scattering processes. Thus, there is a good agreement of the GOA with the reference method for moderate θ_r.

Other comparisons of the second-order contribution $\bar{\sigma}^{\rm tot}_{r,2}$ for all values of ϕ_r (i.e., over the whole upper scattered hemisphere) are plotted in Fig. 9 for H incidence polarization and in Fig. 10 for V incidence polarization, for the same simulations parameters as in Fig. 7. The discretization is 15° for $\phi_r \in [0°; 180°]$ and 5° for $\theta_r \in [-90°; +90°]$. The plus sign indicates the specular direction. It must be noted that the data are not interpolated, even if interpolating should be more relevant to get a more realistic overall representation (especially around $\phi_r = 0$ and $\phi_r = 90°$). The three sub-figures at the top of the figure show the co-polarization, and at the bottom the cross-polarization. Results of $\bar{\sigma}^{\rm tot}_{r,2}$ from the numerical reference method are plotted on the left, from the GOA in the middle, and the difference of the numerical method with the GOA (differences taken in terms of NRCS values in decibels) on the right. The comparisons confirm the good agreement of the GOA with the reference numerical method for moderate scattering angles θ_r.

Fig. 11 presents comparisons for the parameters of Fig. 5, but with an incidence elevation angle $\theta_i = 40°$, an inner relative permittivity $\epsilon_{r2} = 3 + i0.01$, and surfaces with rms slope $\sigma_s = 0.3$. For this configuration, the surfaces have higher rms slopes, which corresponds to the qualitative rms slopes limits of the validity domain of the GOA. Then, the results should highlight limitations of the GOA by comparison with the numerical reference method. It can indeed be seen that contrary to the previous configurations where the cross-polarizations highlight rather good agreement of the GOA for high scattering angles θ_r (especially for VH polarization), in this case the NRCS is always significantly underestimated by the GOA. This can easily be understood: by significantly increasing the rms slopes, the relative

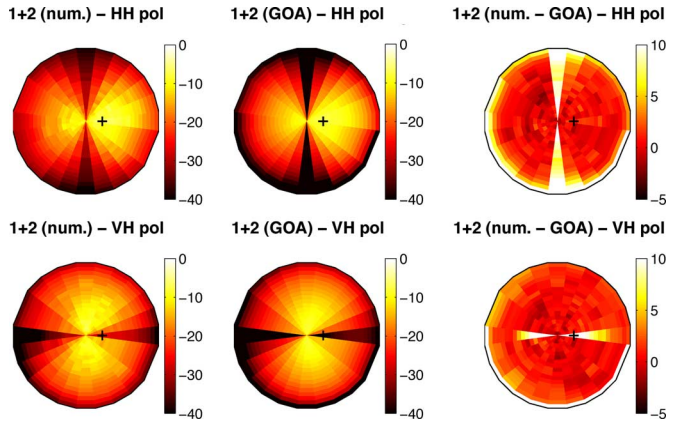

Fig. 9. Same simulations as in Fig. 7, but with an azimuth angle ϕ_r ranging $[0;180]^\circ$, with 15° discretization: Numerical results of $\bar{\sigma}_{r,2}^{\mathrm{tot}}$ for H incidence polarization.

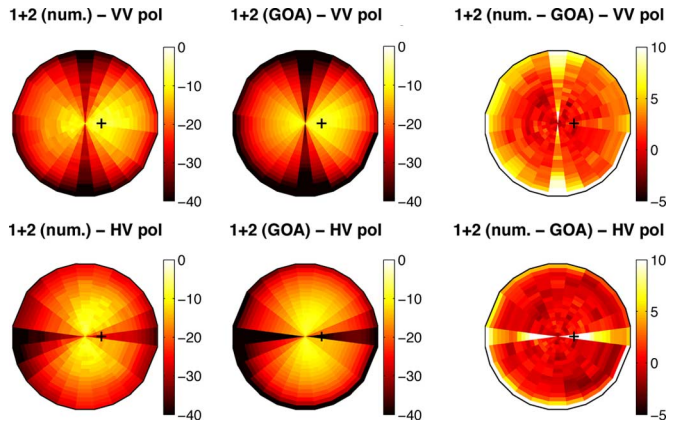

Fig. 10. Same simulations as in Fig. 9, but with V incidence polarization.

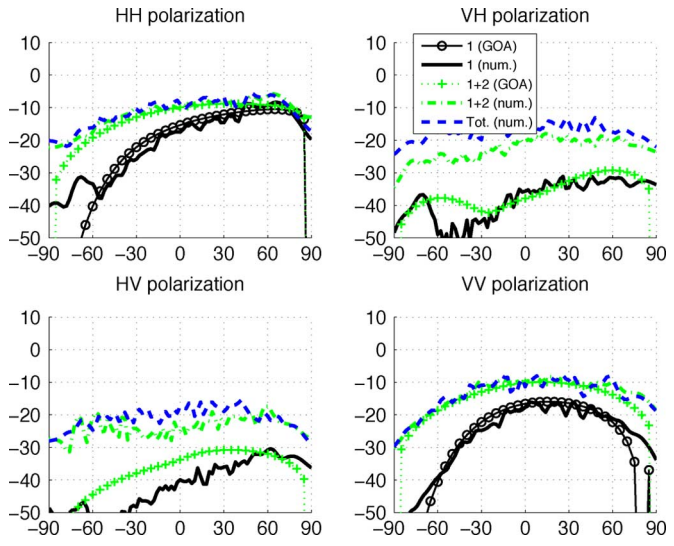

Fig. 11. Same simulations as in Fig. 5, but with an incidence elevation angle $\theta_i = 40^\circ$, an inner relative permittivity $\epsilon_{r2} = 3 + i0.01$, and surfaces with rms slope $\sigma_s = 0.3$.

contribution of the multiple scattering from the same interface effect is increased. For the co-polarizations, the agreement remains good, except for larger θ_r angles. Here, the underestimation by the GOA is a bit more important for grazing θ_r than for the previous cases, mainly owing to the higher rms slopes σ_s.

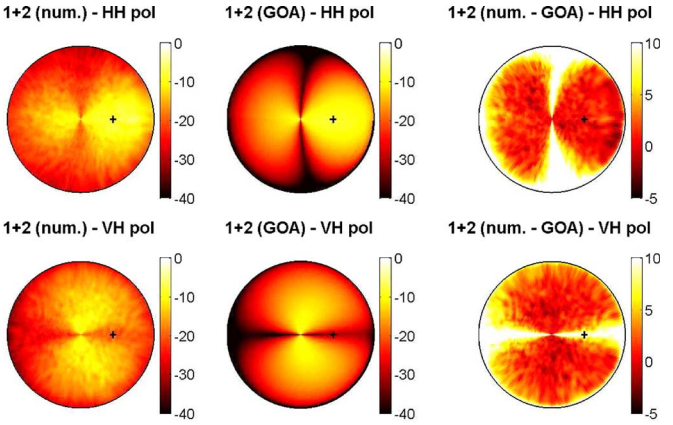

Fig. 12. Same simulations as in Fig. 11, but with an azimuth angle ϕ_r ranging $[0;180]^\circ$, with 2° discretization: Numerical results of $\bar{\sigma}_{r,2}^{\mathrm{tot}}$ for H incidence polarization.

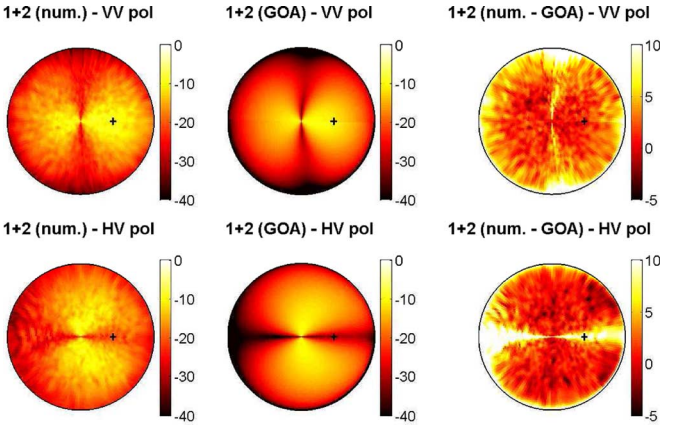

Fig. 13. Same simulations as in Fig. 12, but with V incidence polarization.

Other comparisons of the second-order contribution $\bar{\sigma}_{r,2}^{\mathrm{tot}}$ for various values of ϕ_r are plotted in Fig. 12 for H incidence polarization and in Fig. 13 for V incidence polarization. The discretization is this time 2° for $\phi_r \in [0^\circ; 180^\circ]$ and 2° for $\theta_r \in [-90^\circ; +90^\circ]$, providing a higher resolution image of the bistatic scattering pattern. The comparisons confirm the general good agreement of the GOA with the reference numerical method for moderate scattering angles θ_r. Moreover, limitations of the model are highlighted mainly for grazing θ_r, in and around the in-plane configuration $\phi_r = 0$ for cross-polarizations, and in and around the cross-plane configuration $\phi_r = 90^\circ$ for co-polarizations. It can be noticed that the underestimation by the GOA with shadowing effects is more significant for HH polarization than for VV polarization. Thus, all these comparisons validate the GOA in its validity domain, and help to quantify limitations of the approach for grazing scattering angles and for cross-polarized predictions in the plane of incidence.

V. Conclusion

The GOA with shadowing effects for a rough layer has been extended to a general 3-D problem with 2-D surfaces, allowing it to model more realistic problems and to study the influence

of cross-polarizations. Comparisons with a reference numerical method validated the GOA in its validity domain. The different configurations used confirmed that the model is independent of the layer mean thickness for lossless inner media, and that the model can deal with lossy inner media as well with good predictions. Results showed that for moderate scattering angles, the second-order contribution $\bar{\sigma}_{r,2}^{\mathrm{tot}}$ is generally sufficient to quantify the scattering process. Observed differences of the GOA with the reference method can be attributed primarily to multiple scattering effects on the same interface. As a prospect of this paper, the GOA model for a rough layer could be improved by incorporating multiple scattering effects on the same rough interface, similarly as done by several authors for the double scattering in reflection from a single rough interface [14]–[16].

ACKNOWLEDGMENT

The authors would like to thank the anonymous reviewers for their helpful, relevant, and constructive comments.

REFERENCES

[1] C. Bourlier, G. Berginc, and J. Saillard, "Monostatic and bistatic statistical shadowing functions from a one-dimensional stationary randomly rough surface according to the observation length: I. Single scattering," *Waves Random Media*, vol. 12, no. 2, pp. 145–73, 2002.

[2] N. Pinel, C. Bourlier, and J. Saillard, "Energy conservation of the scattering from rough surfaces in the high-frequency limit," *Opt. Lett.*, vol. 30, no. 15, pp. 2007–2009, Aug. 2005.

[3] N. Pinel, J. Johnson, and C. Bourlier, "A geometrical optics model of three dimensional scattering from a rough surface over a planar surface," *IEEE Trans. Antennas Propag.*, vol. 57, no. 2, pp. 546–554, Feb. 2009.

[4] N. Pinel, N. Déchamps, C. Bourlier, and J. Saillard, "Bistatic scattering from one-dimensional random rough homogeneous layers in the high-frequency limit with shadowing effect," *Waves Random Complex Media*, vol. 17, no. 3, pp. 283–303, Aug. 2007.

[5] A. Fung, *Microwave Scattering and Emission Models and Their Applications*. Boston, MA: Artech House, 1994.

[6] L. Tsang and J. Kong, *Scattering of Electromagnetic Waves, Volume III: Advanced Topics*. New York: Wiley, 2001.

[7] N. Pinel and C. Bourlier, "Scattering from very rough layers under the geometric optics approximation: Further investigation," *J. Opt. Society Amer. A*, vol. 25, no. 6, pp. 1293–1306, Jun. 2008.

[8] K. Pak, L. Tsang, and J. T. Johnson, "Numerical simulations and backscattering enhancement of electromagnetic waves from two dimensional dielectric random rough surfaces with sparse matrix canonical grid method," *J. Opt. Society Amer. A*, vol. 14, no. 7, pp. 1515–1529, 1997.

[9] J. T. Johnson, R. T. Shin, J. A. Kong, L. Tsang, and K. Pak, "A numerical study of the composite surface model for ocean scattering," *IEEE Trans. Geosci. Remote Sensing*, vol. 36, no. 1, pp. 72–83, 1998.

[10] J. T. Johnson, R. T. Shin, J. A. Kong, L. Tsang, and K. Pak, "A numerical study of ocean polarimetric thermal emission," *IEEE Trans. Geosci. Remote Sensing*, vol. 37, no. 1, pt. I, pp. 8–20, 1999.

[11] J. T. Johnson and R. J. Burkholder, "Coupled canonical grid/discrete dipole approach for computing scattering from objects above or below a rough interface," *IEEE Trans. Geosci. Remote Sensing*, vol. 39, pp. 1214–1220, 2001.

[12] J. T. Johnson, "A numerical study of scattering from an object above a rough surface," *IEEE Trans. Antennas Propag.*, vol. 40, pp. 1361–1367, 2002.

[13] J. T. Johnson and R. J. Burkholder, "A study of scattering from an object below a rough interface," *IEEE Trans. Geosci. Remote Sensing*, vol. 42, pp. 59–66, 2004.

[14] A. Ishimaru, C. Le, Y. Kuga, L. Sengers, and T. Chan, "Polarimetric scattering theory for high slope rough surfaces," *Progr. Electromagn. Res.*, vol. 14, pp. 1–36, 1996.

[15] E. Bahar and M. El-Shenawee, "Double-scatter cross sections for two-dimensional random rough surfaces that exhibit backscatter enhancement," *J. Opt. Society Amer. A*, vol. 18, no. 1, pp. 108–16, Jan. 2001.

[16] C. Bourlier and G. Berginc, "Multiple scattering in the high-frequency limit with second-order shadowing function from 2D anisotropic rough dielectric surfaces: I. Theoretical study," *Waves Random Media*, vol. 14, no. 3, pp. 229–52, 2004.

Nicolas Pinel (A'09) was born in Saint-Brieuc, France, in 1980. He received the Engineering degree and the M.S. degree in electronics and electrical engineering both from Polytech'Nantes (Ecole polytechnique de l'université de Nantes), Nantes, France, in 2003 and the Ph.D. degree from the University of Nantes, in 2006.

He is currently working as a contract research Engineer at IREENA Laboratory (Institut de Recherche en Electrotechnique et Electronique de Nantes Atlantique), Nantes. His research interests are in the areas of microwave and optical remote sensing, propagation. In particular, he works on asymptotic methods of electromagnetic wave scattering from rough surfaces and layers, and its application to oil slicks on sea surfaces at moderate and grazing incidence angles.

Joel T. Johnson (F'08) received the Bachelor of Electrical Engineering degree from the Georgia Institute of Technology, Atlanta, in 1991 and the S.M. and Ph.D. degrees from the Massachusetts Institute of Technology, Cambridge, in 1993 and 1996, respectively.

He is currently a Professor in the ElectroScience Laboratory, Department of Electrical and Computer Engineering, The Ohio State University, Columbus. His research interests are in the areas of microwave remote sensing, propagation, and electromagnetic wave theory.

Dr. Johnson is a member of Tau Beta Pi, Eta Kappa Nu, and Phi Kappa Phi and Commissions B and F of the International URSI. He received the 1993 Best Paper Award from the IEEE Geoscience and Remote Sensing Society, was named an Office of Naval Research Young Investigator, received the National Science Foundation Career Award, the Presidential Early Career Award for Scientists and Engineers in 1997, and was recognized by the U.S. National Committee of Union of Radio Science (URSI) as a Booker Fellow in 2002.

Christophe Bourlier (A'08) was born in La Flèche, France, on July 6, 1971. He received the M.S. degree in electronics and the Ph.D. from the University of Rennes, Rennes, France, in 1995 and 1999, respectively.

While at the University of Rennes, he was with the Laboratory of Radiocommunication where he worked on antennas coupling in the VHF-HF band. He was also with the SEI (Système Electronique et Informatique) Laboratory. Now, he is with IREENA Laboratory (Institut de Recherche en Electrotechnique et Electronique de Nantes Atlantique, France) on the Radar team at Polytech'Nantes (University of Nantes, France). He works as an Assistant Researcher of National Center for Scientific Research on electromagnetic wave scattering from rough surfaces and objects for remote sensing applications. He is author of more than 90 journal articles and conference papers.